Effect of the position of constriction on water permeation across a single-walled carbon nanotube

Linsong Wu, Fengmin Wu, Jianlong Kou, and Hangjun Lu*
Department of Physics, Zhejiang Normal University, Jinhua, 321004, China

Yang Liu†
Department of Mechanical Engineering, The Hong Kong Polytechnic University, Hong Kong

(Received 9 January 2011; published 16 June 2011)

The transportation of water across a cell membrane facilitated by water channel proteins is fundamental to the normal water metabolism in all forms of life. It is understood that the narrow region in a water channel is responsible for gating or selectivity. However, the influence of the position of the narrow region on water transportation is still not thoroughly understood. By choosing a single-walled carbon nanotube (SWNT) as a simplified model and using molecular dynamics simulation, we have found that the water flux through the nanotube would change significantly if the narrow location moves away from the middle region along the tube. Simulation results show that the flux reaches the maximum when the deformation occurs in the middle part of nanotube and decreases as the deformation location moves toward the ends of the nanotube. However, the decrease of water flux is not monotonic and the flux gets the minimum near the ends. These interesting phenomena can be explained in terms of water-water interactions and water-SWNT interactions. It can be concluded that the regulation of water transportation through nanopores depends sensitively on the location of the narrow region, and these findings are helpful in devising high flux nanochannels and nanofiltration as well.

DOI: 10.1103/PhysRevE.83.061913 PACS number(s): 87.10.Tf, 66.20.−d, 81.07.De

I. INTRODUCTION

Protein channels, consisting of a pore of minimum radius ∼0.3 nm that spans a lipid bilayer membrane, attract considerable attention due to their varieties of physiological functions in cells [1–3]. It is well known that diverse physiological functions depend on their unique structure and chemical component. Interestingly, in the middle of the channel there is a narrow region responsible for gating or selectivity [1]. A biological system is a perfect system exhibiting harmonization and unification between structure and function. The mechanism of these perfect structures of protein channels is not clear. Recently, a number of experimental and theoretical studies aimed at understanding the mechanisms of water permeation through protein channels at an atomic level were conducted [4–9]. The x-ray crystal structure provides a static picture of a membrane protein channel and provides insight on the working mechanism. Based on the crystal structure, many groups tried to study the dynamical behavior using molecular dynamics (MD) simulation [10,11]. However, how the shape and dimension of the channels regulate the transport of water molecules is not completely understood because of the complicated structure and protein-membrane interactions.

In the past decade, several simplified models of various biological channels have been proposed to explore the influence of geometry, surface character, and flexibility on the ions and water permeation through biological pores, and have gained some useful general consensus on the results [3,12–14]. A carbon nanotube with an appropriate radius is one of the most prominent model systems to consider the perfect structure and some key characteristic of water inside nanotube shared with biological channels, such as the single-file arrangement, wavelike density distribution, and wet-dry transition resulting from confinement [15,16].

Since the first synthesis of the carbon nanotube by Iijima [17], the carbon nanotube has been extensively studied due to its unique mechanical and electronic properties and its atomic smooth inner surface [18–21]. In 2001, Hummer *et al*. showed that a carbon nanotube with a diameter of 8.1 Å could be filled with water despite its strongly hydrophobic character [14]. A minute's change in the nanotube-water interactions could dramatically affect the water occupancy of the channel, inducing two state transitions between empty and filled states [22]. Using a MD simulation, Sansom *et al*. quantified the kinetics of oscillations between a liquid-filled and a vapor-filled pore with radii ranging from 0.35 to 1.0 nm and found that the transition between the empty and filled state depended sensitively on the radius, geometrical structure of the nanotube, and the external charge [3]. In addition, their simulation results indicated that the self-diffusion of water molecules confined in the one-dimensional tube was increased by a factor 2–3 compared with bulk water. The water flow exhibits no friction and is limited primarily by the barriers at the entry and exit of the carbon nanotube [23]. For a carbon nanotube with a radius of 1–2 nm, the water flow rate was more than three orders of magnitude faster than the nonslip, hydrodynamic flow, as calculated from Hagen-Poiseuille equation [24]. Recent simulation results indicated that the unusual enhanced flow rates over Hagen-Poiseuille flow arise from a velocity jump in a depletion region at the water-nanotube interface [25]. So, studying water permeation across the carbon nanotube is of great importance not only for understanding the working mechanism of biological channels but also for the design of molecular sensors, devices, and machines.

In order to study the gating mechanism of biological channels, a single-walled carbon nanotube (SWNT) was used

*zjlhjun@zjnu.cn
†mmyliu@polyu.edu.hk

as a prototype to study the response of the narrow region under continuous deformations by mechanical stress [15]. With simulations, Wan *et al*. found that the nanopore was an excellent nanoscale on-off gate [15]. The flux remained almost fixed within a deformation of 2.0 Å but decreased dramatically for a further deformation of 0.6 Å. The gating of the water permeation across this carbon nanotube was considered to be correlated with the wavelike pattern of water density distribution. Furthermore, by comparing the behavior of water molecules in the 13.4-Å-long tube with that in the 14.6-Å-long tube, we discuss the origin of the wavelike pattern of water density distribution inside the channel and the dependence of the gating effect on the length [26]. A theoretical model has been provided to describe the water density distributions and its change with respect to the deformation of the channel. We found that the wavelike patterns of the water density distributions mainly resulted from the potential barriers at both ends of the nanochannel, together with the tight hydrogen-bonding chain inside the tube.

Some groups [27–29] assigned charges to the atoms of SWNTs or imposed external charge near the atoms of SWNT to mimic a biological channel and found that a similar dipole orientation of water molecules as in aquaporin (AQP) could be generated. Interestingly, our previous work indicated that when a single external charge (of value $+1.0e$) is in the middle region of the SWNT, the nanotube is filled with a single-file water chain. Sharp transitions between empty (closed) and filled (open) states occur once the charge moves away from the middle region [28].

We have known that both the geometrical deformation and the charge position in the middle region of a nanochannel can effectively regulate water permeation, but it is not clear yet what would happen if the gating region moves toward the end of the channel.

In this paper, we choose a 14.8-Å-long SWNT as a model system to investigate what would happen when the narrow region is moved away from the middle region by changing the deformation position along the wall. The detailed simulation methods are introduced in Sec. II. In Sec. III, we present the simulation results and discussion. With simulation, we have found that water permeation across the SWNT depends sensitively on the location of the narrow region. The flux reaches a maximum when the deformation is located just in the middle of nanotube. In addition, the effects of the position of the narrow region on the number of the hydrogen bonds and the flipping frequency of the single-file water chain are studied in Sec. III. Furthermore, we explain the mechanism behind these phenomena in terms of the interaction between the water molecules and carbon atoms on hexagonal network of the SWNT. Finally, conclusions are presented in Sec. IV.

II. SIMULATION METHODS

An uncapped (6,6) SWNT which is embedded along the z direction in two graphite sheets was designed to mimic the dimensions of a biological pore [Fig. 1(a)]. The nanotube is folded by a graphite sheet to a cylinder (156 atoms, 14.8 Å long, and 8.1 Å in diameter). In order to explore the effect of the position of the narrow region on water permeation, one carbon atom (the forced atom) is pushed away from its initial position, resulting in 2.2-Å radial displacement in each simulation system. Consequently, the neighboring atoms are pushed away from the initial positions to form a narrow region in the carbon nanotube because of the bond interactions among the carbon-carbon atoms. Seven different systems were considered by choosing different forced atoms [spheres of the nanotube shown in Fig. 1(a)] in (6,6) SWNT. In order to fix the nanotube in the simulation, each carbon atom in the bottom half of the carbon nanotube is held at its initial position by a restraining force. For the convenience of analysis, the middle carbon atom [the fourth forced atom shown in Fig. 1(a)] is taken as the origin point of the z axis, and the distance between the forced atoms and origin point is denoted by d. Seven forced atoms are symmetrical and the fourth atom is the symmetrical center. The positions of forced atoms indexed from 1 to 7 are -7.4, -4.9, -2.5, 0, 2.5, 4.9, and 7.4 Å, respectively.

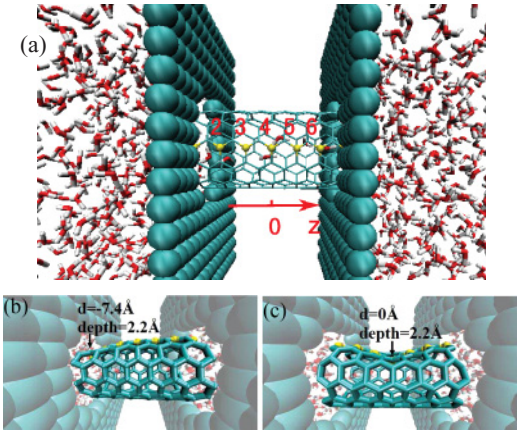

FIG. 1. (Color online) Snapshots of simulation systems. The spheres of the nanotube denote the possible forced atoms and d is the z coordinate of the forced atom. The SWNT in (a) is unperturbed. (b) shows the system for the deformed region locating in left rim of the SWNT ($d = -7.4$ Å). (c) The deformed region is located in the middle of the SWNT ($d = 0$ Å)

The SWNT, together with two graphite sheets, are solvated in a water box, where the TIP3P water model [30] is applied. Water molecules between the two sheets are cleared. The total number of water molecules is 950. The average number of water molecules inside the channel is only ~5.5, much lower than outside the channel. Following the method of Zhu *et al*. [31], we applied an additional acceleration of 0.01 nm ps^{-2} to each water molecule along the $+z$ direction to establish a pressure difference of ~15.7 MPa between the two ends of the nanotube.

MD simulations were performed at a constant particle number, temperature (300 K), and volume (box sizes of $L_x = 3.0$ nm, $L_y = 3.0$ nm, $L_z = 5.0$ nm) with GROMACS 4.0.7 [32]. Berendsen algorithms were applied to simulate at constant temperature (time constant 0.5 ps). A time step of 2 fs was adopted and data were collected every 1 ps. In these simulations, the chosen Lennard-Jones parameters for carbon atoms were $\varepsilon_{C\text{-}C} = 0.3612$ kJ mol^{-1} and $\sigma_{C\text{-}C} = 0.34$ nm. Furthermore, the carbon-water interactions were $\sigma_{CO} = 0.32753$ nm and $\varepsilon_{CO} = 0.47945$ kJ mol^{-1}, respectively. Carbon-carbon lengths of 0.14 nm and bond angles of 120° were maintained by harmonic potentials with spring constants

of 392460 kJ mol^{-1} nm^{-2} and 527 kJ mol^{-1} deg^{-2} before relaxation. The particle-mesh Ewald method [33] was used when computing the long-range electrostatic interactions, and the parameters of the Particle-Mesh Ewald (PME) method included a real space cutoff (1.4 nm), fast Fourier transform (FFT) grid spacing (0.12 nm), fourth-order interpolation, and cutoff distance (1.4 nm). The short-range interactions were computed using a cutoff scheme (cutoff distance, 1.4 nm).

III. RESULTS AND DISCUSSION

Seven sets of simulations ($d = -7.4$, -4.9, -2.5, 0, 2.5, 4.9, and 7.4 Å) were conducted, and each set included eight simulations of 110 ns in duration with different initial states. For each case, the result of the last 105 ns of the simulation was collected for analysis, and the forced atom had a constant deformation depth (radial displacement) of 2.2 Å.

The characteristics of net water flux j for different deformation positions are shown in Fig. 2, where the flux j is defined as the amount of water molecules entering from the left end and leaving at the right end along the $+z$ direction minus the amount of water molecules entering from the right end and leaving at the left end along the $-z$ direction per unit nanosecond. The net water flux is $\sim$14.8 ns^{-1} for the unperturbed SWNT. The W-type profile of water flux shows that the axial position of the deformation plays a key role in regulating water permeation. The net water flux peaks at 12.5 ns^{-1} when the deformation exists in the middle region ($d = 0$ Å) of the SWNT. The flux varies sharply as long as the deformation position moves away from the middle region. Interestingly, the value of the net water flux reaches the minimum if the deformation position is moved from $d = 0$ Å to $d = -4.9$ Å ($\sim$2.5 Å distance from the end of the nanotube), and we call it the corner point of the water flux (shown in Fig. 2). Certainly, we can easily find another corner point at $d = 4.9$ Å symmetrically. It is noteworthy that the net water flux decreases sharply when the deformation position occurs near the end of the SWNT. The flux for $d = -4.9$ Å falls to only approximately one quarter of the flux for $d = 0$ Å, even though the internal volume of the SWNT for $d = -4.9$ Å is obviously larger than that for $d = 0$ Å (see Fig. 1). In other words, the nozzle effect is very important for water permeation. In addition, the results illustrate that the values of the net water flux are not fully symmetrical, even though the deformation positions are symmetrical at approximately $d = 0$ Å [see Figs. 2 and 1(a)]. For example, the net water flux for $d = -4.9$ Å (3.5 ns^{-1}) is obviously smaller than that for $d = 4.9$ Å (5.1 ns^{-1}). Meanwhile, the net water fluxes for $d = -7.4$ and 7.4 Å also exhibit similar behavior and their values are 6.4 and 7.0 ns^{-1}, respectively. The current simulation results agree with the previous work [34], in which liquid flows more easily along the convergent direction than along the divergent one.

Then a question arises: Why is the location of the narrow portion of the pore so important? To understand thoroughly the mechanism, we first compute the potential of mean force (PMF), which is often used to characterize the mobility of the water molecules inside the nanotube [35]. The single-file water chain confined in the SWNT hops through a series of free-energy barriers in a concerted fashion, therefore the height of the free-energy barriers remarkably influence the water

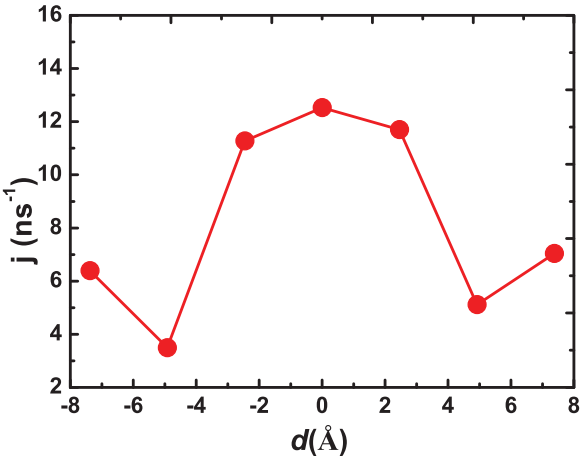

FIG. 2. (Color online) The water flux across the SWNT for different deformation positions d.

permeation through the SWNT. The water translocation time would increase with increasing the crests and the peak-peak distance [35].

Figures 3(a) and 3(b) show variations of the PMF along the axis of the tube for each situation. It can be seen that deformation leads to an increase in the height of the free-energy barriers and the peak-peak distance of the free energy. With moving the deformation position along the z axis (nanotube axis), the PMF curves also have a corresponding translation. It is obvious that the PMF curves jump remarkably near the deformation positions, especially when the deformation positions are located near the rims of the tube. Water molecules must climb higher free-energy barriers if they permeate through these kinds of deformation regions. The numerical results indicate that the free-energy barrier increase much more for $d = -4.9$ and 4.9 Å than those for the other five situations, therefore they would induce corner points at $d = -4.9$ and 4.9 Å. The crest of the curve near the deformation region for $d = -4.9$ Å is higher than that for $d = 4.9$ Å. In other words, water molecules have more difficulty passing through this narrow region when it is located at $d = -4.9$ Å. Correspondingly, the flux for $d = -4.9$ Å is smaller than that for $d = 4.9$ Å.

To better understand why the location of the narrow portion plays a key role in water transportation through the nanotube, we calculate the total interaction potential (it is denoted by the symbol P in this paper) of the confined water inside the SWNT. In this work the potential includes two parts: One is the

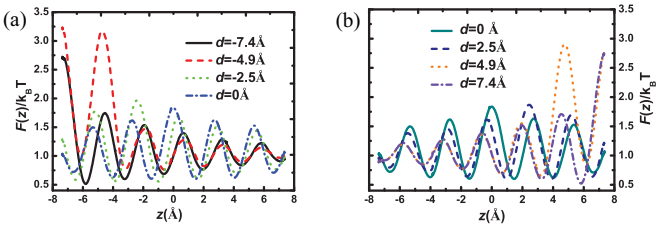

FIG. 3. (Color online) The profile of potential of mean force (PMF) along the SWNT for different d. PMF, $F(z)$, is calculated from the equilibrium water probability density $\rho(z)$ by $F(z) = -k_B T \ln \rho(z)$ [36,37].

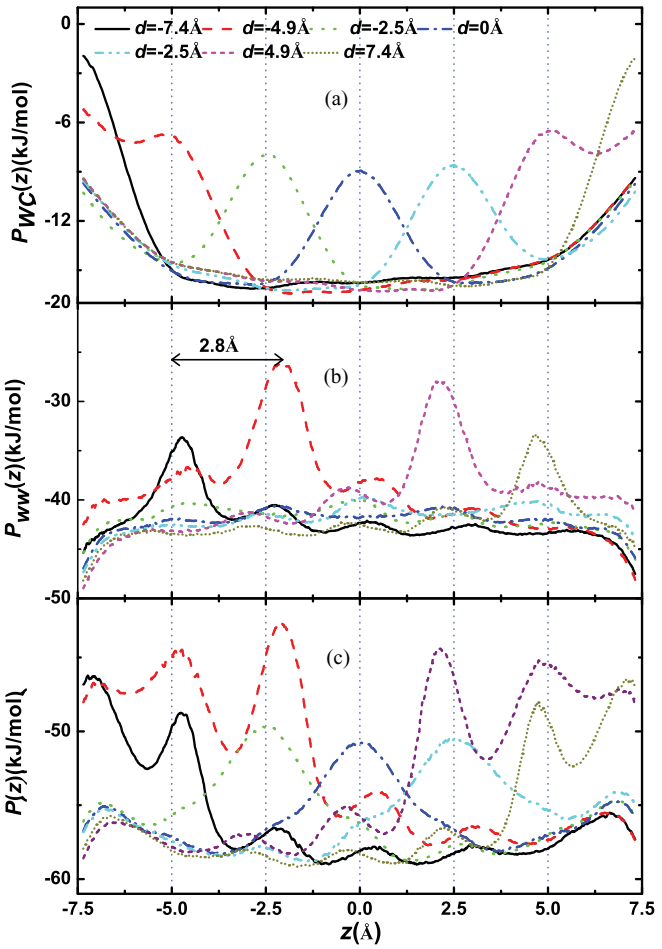

FIG. 4. (Color online) (a)–(c) The average water-SWNT, water-water, and the total interaction potentials along z for different d, respectively.

water-water interactions (the interaction energies of the water molecule at position z inside the SWNT with its neighboring water molecules), denoted by P_{WW}, and the other part is the water-SWNT interactions (the interactions of the confined water at position z with the carbon atoms of SWNT), denoted by P_{WC}. The results are shown in Fig. 4. The potential energy curve of P_{WC} for the unperturbed SWNT has a symmetrical "U-like" shape, and the lowest is located in the middle of the SWNT (the position of $z = 0$ Å) [26]. In line with intuition, when the SWNT is narrowed at d, the potential barrier appears at $z = d$ (the position of the narrowest portion of the SWNT). The profile of the curve of P_{WC} changes from a "U-like" shape into a "W-like" shape [see Fig. 4(a)]. As the location of the narrow portion moves to the ends of the nanotube, the peak of P_{WC} moves to the ends of the nanotube correspondingly, and the height of the peak increases due to a "U-like" shape of P_{WC} for the unperturbed SWNT.

It is known that water molecules inside the SWNT are usually tightly connected by hydrogen bonds. For $|d| \leqslant 2.5$ Å, the water-SWNT interaction potential P_{WC} is not enough to break the hydrogen-bonding chain structure inside the SWNT. However, for $|d| \geqslant 4.9$ Å, the possibility of breaking the hydrogen bond increases dramatically because of a sharp increase in P_{WC} ($z = d$). Figure 4(b) shows that P_{WW} for $d = -4.9$ Å reaches maximum at $z = -2.1$ Å, which is ~2.8 Å away from the deformed position of $z = d = -4.9$ Å, indicating that the water molecule at $z = -2.1$ Å usually loses one hydrogen bond. Note that, for $d = -4.9$ Å, the value of P_{WW} ($z = -4.9$ Å) is lower than that of P_{WW} ($z = -2.1$ Å). This is because the possibility of the water molecule being located in $z = -2.1$ Å is larger than in $z = -4.9$ Å, resulting from P_{WC} ($z = -4.9$ Å) > P_{WC} (-2.1 Å). Certainly, the average number of the hydrogen bonds of the water molecule at $z = -2.1$ Å is more than that of the water molecule at $z = -4.9$ Å. In other words, when there is a water molecule located nearly in $z = -4.9$ Å, usually there exist water molecules in two sides of it (near $z = -2.1$ Å and $z = -7.7$ Å), rather than vice versa. From Fig. 4(b), we can find that P_{WW} ($z < -4.9$ Å) is not the same as P_{WW} ($z > -4.9$ Å). The main reason is that the water molecules in the region of $z < -4.9$ Å are closer to the bulk water than those in the region of $z > -4.9$ Å. The same mechanism (water molecules near $z = -7.9$ Å are closer to the bulk water than those near $z = -4.9$ Å) makes that the height of the peak of P_{WW} for $d = -7.4$ Å is lower than that for $d = -4.9$ Å.

The total interaction potential $P(z)$ can be calculated by $P(z) = P_{WC}(z) + P_{WW}(z)$. Figure 4(c) shows the variation of the total interaction potential along the tube. For the cases of $d = -7.4$, -4.9, 4.9, and 7.4 Å, the distributions $P(z)$ seem to be lifted up. The wavelike pattern for $d = 0$ Å is lifted less than the others, which results in the largest net flux. Moreover, the maximum total interaction potentials exist in the systems of $d = -4.9$ and 4.9 Å. Correspondingly, the net water flux in these two systems is small. Therefore, we find that the net water flux is mainly controlled by the water-water interaction and water-carbon interaction. The different position of the narrow region results in a change of the total interaction potential.

ΔP, the difference between the maximum and minimum of the interaction potential, is usually used to characterize the potential profile. It was calculated and plotted as black filled circles in the inset of Fig. 5. When d is zero (the narrow portion

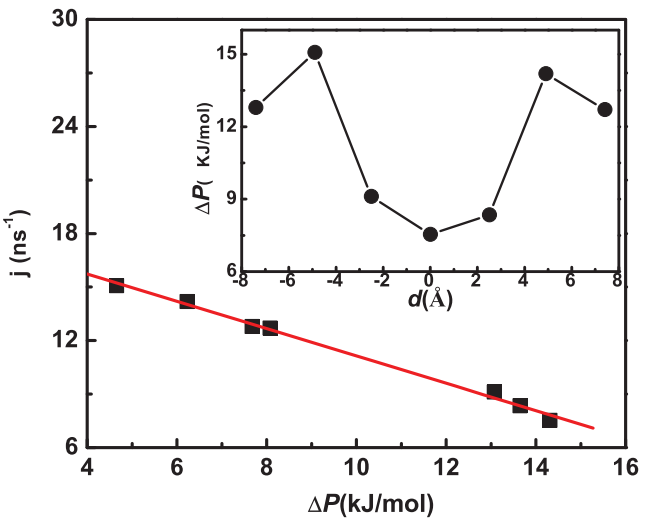

FIG. 5. (Color online) The difference between the maximum and minimum of the interaction potential ΔP and the relationship between ΔP and the net water flux for different d. The solid line is a linear fit.

locates in the middle of the SWNT), ΔP is ~7.7 kJ mol^{-1}, only half of the ΔP for $d = -4.9$ or 4.9 Å. Consequently, the flux for $d = 0$ Å is the maximum. Figure 5 shows the relationship between the water flux and ΔP for all different positions of the narrow portion shown in Fig. 5. The water flux decreases almost linearly with increasing ΔP, and the data can be well fitted by the following formula:

$$j = j_0(1 - \Delta P/\varepsilon),$$

with $\varepsilon \approx 18.1$ kJ mol^{-1} and $j_0 = 21.7$ ns^{-1}, indicating a strong dependence of flux on ΔP. It should be noted that ΔP in this paper is different from ΔP_{WS} in Ref. [16]. In our study, P includes not only the water-SWNT interaction but also the water-water interaction. ΔP is the difference between the maximum and minimum of the total interaction potential. According to the above fitted formula, the net water flux would be decreased to zero when $\Delta P = \varepsilon \approx 18.1$ kJ mol^{-1}. To check the validity of the prediction, we set a system of depth = 2.3 Å and $d = -4.9$ Å, and then the simulation result shows that the net water flux is still ~0.6 ns^{-1} and the matching ΔP is ~22 kJ mol^{-1}, implying that the fitted linear law is a good fit only for $\Delta P < 16$ kJ mol^{-1}.

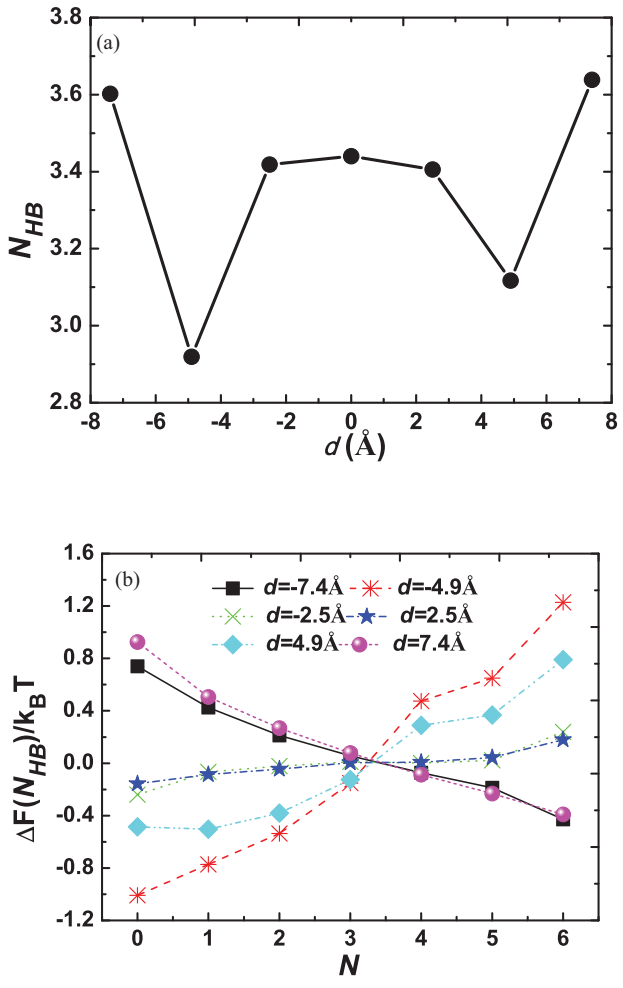

FIG. 6. (Color online) (a) The average number of hydrogen bonds between water molecules inside the SWNT for different d. (b) The free-energy difference $\Delta F(N_{HB})$ for different d, where $\Delta F(N_{HB})$ is equal to $[-\ln p(N_{HB})_d] - [-\ln p(N_{HB})_{d=0}]$.

It has been recognized that the tight hydrogen-bonding chain connecting water molecules inside the nanotube plays a key role in the movement of water molecules along the quansi-one-dimensional (6,6) SWNT axis stochastically and concertedly [14]. Figure 6(a) shows the variation of the average hydrogen-bond number with the deformation position. When d is zero, the average number of hydrogen bonds is ~3.4, more than the case of $d = \pm 4.9$ Å but less than the case of $d = \pm 7.4$ Å. Figure 6(b) illustrates the free energy of the hydrogen-bond number fluctuations $F(N_{HB})/k_BT = -\ln p(N_{HB})$, where $p(N_{HB})$ is the probability of finding exactly N hydrogen bonds connecting the water molecules inside the SWNT. To analyze conveniently the hydrogen-bond number fluctuations, we define the difference as $\Delta F(N_{HB})$. Its value is equal to $[-\ln p(N_{HB})_d] - [-\ln p(N_{HB})_{d=0}]$. The vertical coordinate represents the number of the hydrogen bonds connecting the water molecules inside the SWNT. It can be seen that the hydrogen bonds are affected by changing the deformation position. The probability of $N_{HB} < 3$ in the system of $d = 0$ Å is obviously smaller than those of other systems except for systems of $d = -7.4$ and 7.4 Å. In other words, the probability of emerging in an empty state in the system of $d = 0$ Å is less than those for other systems. Correspondingly, the probability of $N_{HB} > 3$ is larger, therefore, the probability of inducing a filled state is higher, and the net water flux is matching higher. In systems of $d = -7.4$ and 7.4 Å, it is interesting to note that there is a larger probability of inducing a filled state than the system of $d = 0$ Å, but the matching net water flux is still lower than that of the system of $d = 0$ Å. This phenomenon can be understood in that the water molecules can easily enter the tube from the undeformed side, but it is difficult for them to pass through the high free-energy region (shown in Fig. 3)—then the staying time will be obviously longer, and therefore the probability for $N_{HB} > 3$ is larger in these two systems.

An important feature of the hydrogen bond is its directionality. Hydrogen bonds in the SWNT are highly oriented and nearly aligned along the nanochannel axis, and they collectively flip their orientations due to ambient noise. We quantify the orientation of a water chain by defining a characteristic angle denoted by $\bar{\phi}$, where ϕ is the angle between the dipole of a water molecule at position z inside the SWNT and the z axis (nanotube axis), and taking an average over all the water molecules inside the nanotube, where the average covers all the water molecules inside the tube. As described in our previous papers [15,26], $\bar{\phi}$ falls into two ranges, i.e., $15^\circ < \bar{\phi} < 50^\circ$ and $130^\circ < \bar{\phi} < 165^\circ$. If we define a flip as $\bar{\phi}$ passing through 90°, we can compute the number of flips per nanosecond, denoted by the flipping frequency f_{flip}. As shown in Fig. 7, the flipping frequency is ~0.06 ns^{-1} for an unperturbed nanotube which is remarkably lower than 0.5 ns^{-1} for SWNT immersed in bulk water [14], and it agrees well with Ref. [16] in which the water molecules were cleared between the sheets and the length of the carbon nanotube was longer. Figure 7 also shows the variation of flipping frequency with different positions of narrow region d. The flipping frequency is 0.078 ns^{-1} for $d = -7.4$ Å and 0.08 ns^{-1} for $d = 7.4$ Å, close to the flipping frequency for the unperturbed nanotube. However, the water flux is very small, only 6.4 and 7.0 ns^{-1}, respectively. For $d = -7.4$ Å the water molecules penetrate

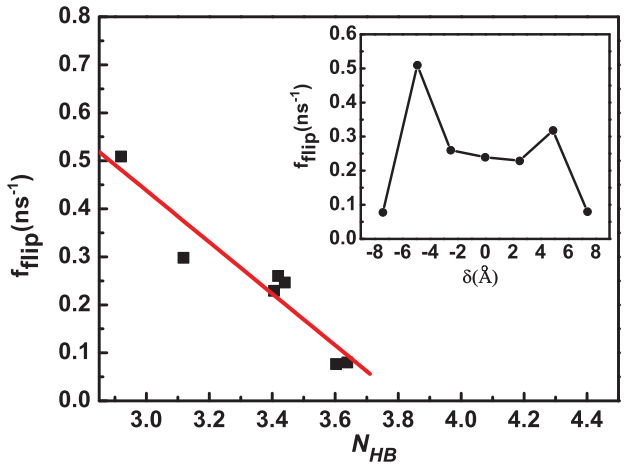

FIG. 7. (Color online) The flipping frequency for different d and the relation between flipping frequency and average hydrogen-bond number. The solid line is a linear fit.

the nanotube more easily from the right, and there is usually an unoccupied site near the narrowed left rim, resulting in shielding from the fluctuation induced by the remaining bulk water. Therefore, it is difficult for the water molecules to be transported through the deformed left rim, consequently the flux decreases drastically and the flipping of the water dipoles is more difficult than those of other cases. There is a similar mechanism for $d = 7.4$ Å.

We note that the maximum of the flipping frequency is 0.51 ns^{-1} for $d = -4.9$ Å, which is obviously larger than the flipping frequency for $d = 4.9$ Å. Even though the deformation positions of the two systems are symmetrical, the difference of the flipping frequency reaches up to 0.19 ns^{-1}. The flipping activation is mainly induced by the hydrogen-bond defect along the water chain and the ambient fluctuation. Certainly the fluctuation is induced by the bulk water near the rims of the nanotube [38]. To better understand why the flipping frequency for $d = \pm 4.9$ Å is larger than the others and what induces their asymmetry, we further analyze the structure of the water chain inside the nanotube for two cases. Figure 8 shows two snapshots of the simulation results. We define the region near the forced atom as the deformed region, which usually induces a defect in the water chain. In contrast to the cases for $d = \pm 7.4$ Å, there often exists a water molecule inside the rim of the nanotube connecting with the bulk water molecules outside. The deformed region induces the breakage of hydrogen bonds inside the nanotube and does not shield the fluctuation from the bulk water effectively because of the water molecule in the rim of the nanotube. Therefore, the flipping frequency becomes large.

For $d = \pm 7.4$ Å, these two symmetrical systems can also be understood to have the symmetric deformation position, but their directions of the pressure gradient are opposite. So the results show that the direction of the pressure gradient could well affect the water permeation. In this work, the pressure difference is fixed and the direction is always from $-z$ to $+z$. Comparing to the system of $d = -4.9$ Å, there is a similar probability of an emerging hydrogen-bond defect in right side of the tube in the system of $d = 4.9$ Å. To some extent, the pressure difference prevents the defect from

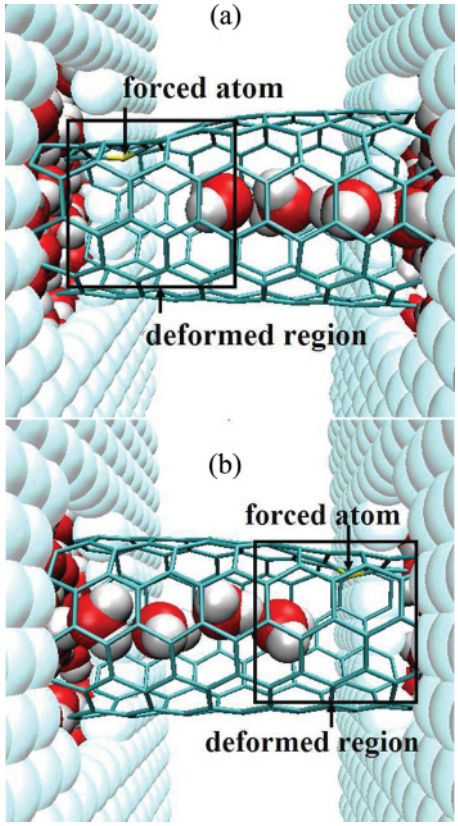

FIG. 8. (Color online) Snapshots of MD simulation (a) for $d = -4.9$ Å and (b) for $d = 4.9$ Å

getting into the tube from the right side, and the corresponding flipping frequency is smaller than that of $d = -4.9$ Å. So there are different flipping frequencies in these two symmetrical systems.

Figure 7 gives the relationship between the flipping frequency and the number of hydrogen bonds. The dipole flip of the ordered water chain inside the SWNT is the process where the hydrogen-bonding defect moves through the tube [38]. The defect in the water chain plays a key role in dipole flipping. The number of hydrogen bonds reflects the probability of defects of the water wire. The average number of hydrogen bonds [N_{HB} for an unperturbed carbon nanotube (14.8 Å long)] is ~3.8 ($N_{HB0} = 3.8$). The average number of defects is approximately equal to $N_{HB0} - N_{HB}$. As the number of hydrogen bonds is only 2.9, the flipping frequency is 0.51 ns^{-1}. With increasing the number of hydrogen bonds to 3.6, the flipping frequency decreases to 0.078 ns^{-1}. The function

$$f_{flip} = f_{flip0}(1 - N_{HB}/N_{HB0})$$

can fit the data quite well, where $N_{HB0} \approx 3.8$ and $f_{flip0} = 2.1$ ns^{-1}. This linear relationship indicates that the defects in the water chain lead to an increase in the flipping frequency by breakage of hydrogen bonds inside the nanotube.

IV. CONCLUSIONS

Molecular dynamics simulations are carried out to systematically elaborate the effect of a narrow portion on water

permeation through a nanotube. Simulation results indicate that the water flux and dipole flipping frequency of the water chain is significantly influenced by the location of the deformation. Interestingly, when the deformation is located in the middle of the nanotube, the water flux across the nanotube reaches a maximum, suggesting that the hourglass shape is more convenient for water molecules to pass through the nanotube than a funnel shape. Note that the depth of the deformation for all cases is 2.2 Å and the decrease of the volume for $d = 0$ Å (deformation locating in the middle part) is larger than those of the other cases.

The effect of the location of the deformation on the water transport can be understood using PMFs along the tube axis and interaction potentials. The water flux and dipole flipping frequencies are regulated mainly by the PMF and interaction potentials near the narrowed region. Obviously, the peak of the water-SWNT interaction potential increases as the narrow location moves away from the middle region along the nanotube. Correspondingly, the water-water interaction potential increases because the hydrogen bond is usually interrupted due to an increase of the water-SWNT interaction potentials. However, when the deformed position is just located in one of the two ends of the SWNT, the water-water interaction potential decreases since the bulk water near the entrances of the SWNT are not affected by the deformation of the nanotube. Therefore, the peak of the total interaction potential increases as the deformation location moves to the ends of the nanotube, but the increase is not monotonic and the peak reaches the highest levels near the ends. The axial position of the deformed region has a significant influence on the interaction potentials, PMF, and the water flux.

We use the difference between the maximum and minimum of the interaction potential ΔP to characterize the potential profile. It is found that the number of the hydrogen bonds decreases as ΔP increases. Correspondingly, the water flux across the nanotube decreases linearly. The dipole flipping frequency increases as the number of the hydrogen bonds decreases. The main reason for the breakage of hydrogen bonds in a water chain inside the nanotube is the water-SWNT interaction potential. The defect induced by the breakage of the hydrogen bond inside the nanotube, together with the fluctuation induced by the bulk water molecules outside the nanotube, are responsible for the dipole flip of the water chain.

The current research may be helpful in designing high flux nanofiltration tools and understanding the effects of the complex shapes and structures of biological channels on water permeation.

ACKNOWLEDGMENTS

We gratefully acknowledge valuable discussion with Penger Tong, Peng Xiu, and Zaixing Yang. This work is supported by Zhejiang Provincial Natural Science Foundation of China Grants No. Y6100384 and No. Z6090556, the National Natural Science Foundation of China Grant No. 11005093, and the Hong Kong Polytechnic University Grant No. G-YG84.

[1] K. Murata, K. Mitsuoaka, T. Hirai, T. Walz, P. Agre, J. B. Heymann, A. Engel, and Y. Fujiyoshi, Nature (London) **407**, 599 (2000).
[2] Y. Fujiyosh, K. Mitsuoka, B. L. de Groot, A. Philippsen, H. Grubmüller, P. Agre, and A. Engel, Curr. Opin. Struct. Biol. **12**, 509 (2002).
[3] O. Beckstein and M. S. P. Sansom, Proc. Natl. Acad. Sci. U.S.A. **100**, 7063 (2003).
[4] H. X. Sui, B. G. Han, J. K. Lee, P. Walian, and B. K. Jap, Nature (London) **414**, 872 (2001).
[5] M. O. Jensen, E. Tajkhorshid, and K. Schulten, Biophys. J. **85**, 2884 (2003).
[6] M. S. P. Sansom and R. J. Law, Curr. Biol. **11**, R71 (2001).
[7] M. Hashido, A. Kidera, and M. Ikeguchi, Biophys. J. **93**, 373 (2007).
[8] B. Liu, X. Y. Li, B. L. Li, B. Q. Xu, and Y. L. Zhao, Nano Lett. **9**, 1386 (2009).
[9] B. L. Groot and H. Grubmüller, Science **294**, 2353 (2001).
[10] M. Jensen, S. Park, E. Tajkhorshid, and K. Schulten, Proc. Natl. Acad. Sci. U.S.A. **99**, 6731 (2002).
[11] F. Q. Zhu, E. Tajkhorshid, and K. Schulten, Biophys. J. **86**, 50 (2004).
[12] X. J. Gong, J. C. Li, K. Xu, J. F. Wang, and H. Yang, J. Am. Chem. Soc. **132**, 1873 (2010).
[13] B. Corry, J. Phys. Chem. B **112**, 1427 (2008).
[14] G. Hummer, J. C. Rasaiah, and J. P. Noworyta, Nature (London) **414**, 188 (2001).
[15] R. Z. Wan, J. Y. Li, H. J. Lu, and H. P. Fang, J. Am. Chem. Soc. **127**, 7166 (2005).
[16] X. Gong, J. Li, H. Zhang, R. Wan, H. Lu, S. Wang, and H. Fang, Phys. Rev. Lett. **101**, 257801 (2008).
[17] S. Iijima, Nature (London) **354**, 56 (1991).
[18] N. Naguib, H. Ye, Y. Gogotsi, A. G. Yazicioglu, C. M. Megaridis, and M. Yoshimura, Nano Lett. **4**, 2237 (2004).
[19] H. Ye, N. Naguib, Y. Gogotsi, A. Yazicioglu, and C. M. Megaridis, Nanotechnology **15**, 1 (2004).
[20] Y. Gogotsi, J. Libera, A. G. Yazicioglu, and C. M. Megaridis, Appl. Phys. Lett. **79**, 1021 (2001).
[21] K. Koga, G. T. Gao, H. Tanaka, and X. C. Zeng, Nature (London) **412**, 802 (2001).
[22] A. Waghe, J. C. Rasaiah, and G. Hummer, J. Chem. Phys. **177**, 10789 (2002).
[23] A. Kalra, S. Garde, and G. Hummer, Proc. Natl. Acad. Sci. U.S.A. **100**, 10175 (2003).
[24] J. K. Holt, H. G. Park, Y. M. Wang, M. Stadermann, A. B. Artyukhin, P. C. Grigoropoulos, A. Noy, and O. Bakajin, Science **312**, 1034 (2006).
[25] S. Joseph and N. R. Aluru, Nano Lett. **8**, 452 (2008).
[26] H. Lu, J. Li, X. Gong, R. Wan, Z. Li, and H. Fang, Phys. Rev. B **77**, 174115 (2008).

[27] F. Q. Zhu and K. Schulten, Biophys. J. **85**, 236 (2003).
[28] J. Y. Li, X. J. Gong, H. J. Lu, D. Li, H. P. Fang, and R. H. Zhou, Proc. Natl. Acad. Sci. U.S.A. **104**, 3687 (2007).
[29] H. J. Lu, X. Y. Zhou, F. M. Wu, and Y. S. Xu, J. Phys. Chem. B **112**, 16777 (2008).
[30] W. L. Jorgensen, J. Chandrasekhar, J. D. Madura, R. W. Impey, and M. L. Klein, J. Chem. Phys. **79**, 926 (1983).
[31] F. Q. Zhu, E. Tajkhorshid, and K. Schulten, Biophys. J. **83**, 154 (2002).
[32] D. van der Spoel, E. Lindahl, B. Hess, G. Groenhof, A. E. Mark, and H. J. C. Berendsen, J. Comput. Chem. **26**, 1701 (2005).
[33] E. Lindahl, B. Hess, and D. van der Spoel, J. Mol. Model. **7**, 306 (2001).
[34] M. Chinappi, E. Angelis, S. Melchionna, C. M. Casciola, S. Succi, and R. Piva, Phys. Rev. Lett. **97**, 144509 (2006).
[35] S. Andreev, D. Reichman, and G. Hummer, J. Chem. Phys. **123**, 194502 (2005).
[36] I. Kosztin, B. Barz, and L. Janosi, J. Chem. Phys. **124**, 064106 (2006).
[37] D. Frenkel and B. Smit, *Understanding Molecular Simulation: From Algorithms to Applications* (Academic, San Diego, CA, 1996).
[38] R. B. Best and G. Hummer, Proc. Natl. Acad. Sci. U.S.A. **102**, 6732 (2005).